Vol. 85 (1994) *ACTA PHYSICA POLONICA A* No. 5

TRANSMISSION ELECTRON MICROSCOPY STUDIES OF Kr^+-IMPLANTED SILICON

J. MORAWIEC

Institute of Physics, Polish Academy of Sciences
Al. Lotników 32/46, 02-668 Warszawa, Poland

(Received April 30, 1993, revised version January 20, 1994)

The structure and the depth distribution of radiation damage caused in ⟨111⟩ Si by high-dose krypton implantations (E_i = 150 keV, T_i = RT, $D_1 = 5 \times 10^{15}$, $D_2 = 1 \times 10^{16}$ and $D_3 = 5 \times 10^{16}$ cm^{-2}) have been investigated using techniques of transmission electron microscopy. Formation of secondary defects (Kr bubbles and microtwins) on subsequent different annealing procedures, i.e. during solid phase epitaxial regrowth of damaged layers by conventional furnace heating and liquid phase epitaxial regrowth by applying laser pulses is compared and discussed.

PACS numbers: 61.16.Bg, 61.72.Ff, 61.72.Qq, 61.72.Tt, 68.35.Fx, 81.40.Gh

1. Introduction

The aim of this work was to study structural changes of single-crystal silicon induced by high-dose Kr^+-implantation using transmission electron microscopy (TEM).

Both the primary implantation damage and extended defects formed in a restored structure during subsequent annealing were analyzed as a function of a certain dose. Two heating procedures, that is furnace and laser annealing, were applied under chosen conditions to study effects of solid vs. liquid phase epitaxial regrowth (SPEG vs. LPEG) of damaged layers [1].

2. Experimental

At room temperature and at an energy of 150 keV, ⟨111⟩ dislocation-free and not initially-doped silicon wafers were implanted with $^{84}Kr^+$ ions using three different doses: $D_1 = 5 \times 10^{15}$, $D_2 = 1 \times 10^{16}$ and $D_3 = 5 \times 10^{16}$ ions per cm^2. The ion bombardments were performed with the silicon targets slightly tilted (approximately 7°) from on-axis ⟨111⟩ direction to avoid channeling effects. These implantation conditions corresponded to an LSS (Lindhard, Scharff, Schiott) theoretical projected range of 78.8 nm with straggling of 26.6 nm [2].

The irradiated wafers were furnace annealed at 800°C for 3 h in vacuum (10^{-3} Pa). The second annealing method applied ruby laser pulses ($W \cong 1.5$ J/cm^2, $t = 20$ ns).

To prepare planar and cross-sectional samples, standard chemical polishing (from the back side) and "face-to-face" ion milling methods, respectively, were used [3, 4].

The TEM studies were carried out in high resolution JEM 2000EX and high voltage JEM 1000 electron microscopes.

3. Results and analysis

3.1. Primary damage

Implantation using three different doses results in the total amorphization of irradiated surface layers (see the micrographs in the central column in Fig. 1).

What should be pointed out here is the effect of the D_3 dose which causes swelling of the irradiated layer, thus leading to significantly thicker effective amorphization (approximately $3R_p$, R_p stands for projected range) than the two lower doses (approximately $2R_p$ in both cases). Moreover, in the swelled amorphized material of the D_3 implant a bubble-like structure is detected at the depth of R_p (as seen in a micrograph illustrating the primary damage of the dose).

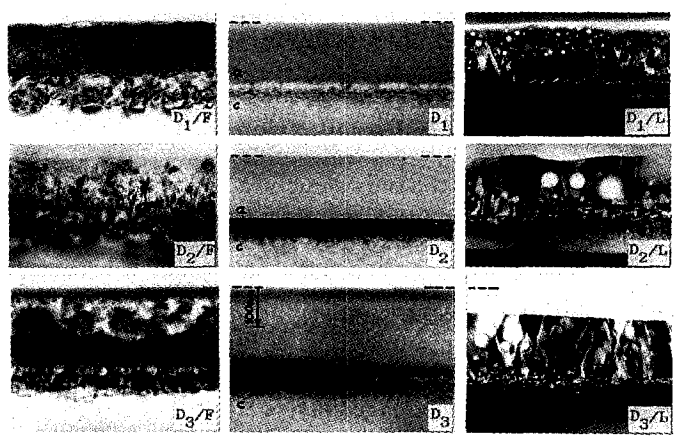

Fig. 1. Set of micrographs showing primary implantation damage (central column) and the distribution of secondary defects in layers recrystallized during furnace (column on the left) and laser (on the right) annealing (equally magnified bright field (BF) images).

The visible "a/c" interfaces between amorphized silicon (marked by "a") and undamaged crystalline matrix (marked by "c") consist of very small isolated disordered zones and structural "end-of-range" defects created on dynamic annealing [5, 6].

3.2. Recrystallization and secondary defects

The set of micrographs in Fig. 1 presents results of annealing experiments. During heat treatment by the above two procedures damaged layers undergo epitaxial regrowth. In each case, at about the depth of "end-of-range" the recrystallization front starting at the (111)-oriented a/c interface, leaves behind a thin ($\approx$ 30 nm) band of small interstitial Frank loops. Characteristic and common post-annealing defects, that is krypton precipitates (gas/fluid filled bubbles) and microtwins with boundaries along {111} planes, are found to be further developed toward the surface. However, this secondary defect structure is far more dense after furnace annealing (see micrographs in the left column) rather than after laser annealing (micrographs on the right). Though krypton bubbles formed during furnace heating are hardly seen through high-density microtwins in micrographs in Fig. 1, they are clearly revealed by using the high-order reflection diffraction contrast technique (see Fig. 2 and its description).

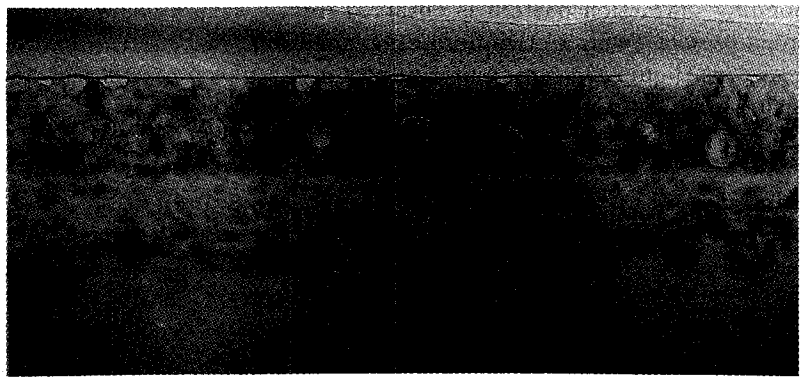

Fig. 2. Bubbles — marked by arrows — formed at the surface with inert gas atoms trying to out-diffuse but trapped by an oxide film (the main population of Kr precipitates is visible at the depth of maximum impurity concentration ($\approx R_p$)) (BF high-order 220 reflection micrograph).

3.2.1. Solid phase epitaxial regrowth (SPEG)

The characteristic effect of regrowth during furnace heating is that in spite of a long heat treatment recrystallization is not fully completed for all doses used. This is easily seen for the D_3 dose (see micrograph D_3/F, where F stands for furnace annealing) where twin-growth is stopped by an existing barrier — a band of Kr bubbles concentrated around a depth of R_p. Above this depth only separated silicon polycrystallites are formed within the surface layer which consists of residual amorphous material and extended krypton bubbles. For the two lower doses D_1 and D_2 (micrographs D_1/F and D_2/F) regrowth is also interrupted and finishes with the nucleation of the polycrystalline phase, however, much closer to or in the very vicinity of a surface.

Finally, it should be noticed that there are still high internal strains after furnace treatment at a depth of end-of-range, resulting in plastic deformation by the generation of misfit-type dislocations.

3.2.2. Liquid phase epitaxial regrowth (LPEG)

Contrary to furnace heating, laser annealing leads to the complete from-the--melt recrystallization of damaged layers, and it is successful at least for D_1 and D_2 implants (the observed effect of the hillock surface morphology hints at the ripple-formation during melting). In a sample implanted with a rather destructive dose D_3 the loss of the surface layer down to a depth of approx. R_p is observed (compare the surface levels before and after laser annealing in micrographs D_3 and D_3/L, where L stands for laser heating). Certainly, structural discontinuity, that is Kr precipitation, occurring at the critical depth R_p of primary damage (see micrograph D_3) favours this behaviour.

Examples of typical secondary defects found in restored structures after laser annealing are shown in high-resolution ⟨110⟩ projections:

– microtwins reaching without restraint the surface (Fig. 3, in the inset a corresponding diffraction pattern is obtained from a somewhat larger area with extra spots present owing to twin formation on {111} planes [7]),

– gaseous (liquid ?) krypton precipitates in the silicon matrix (considered to be quench-in defects formed during cooling-down the melt), (Fig. 4).

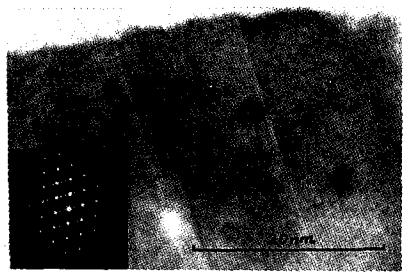

Fig. 3

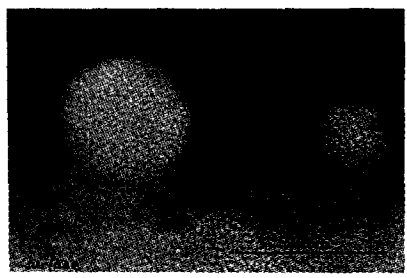

Fig. 4

Fig. 3. ⟨110⟩ lattice image of microtwins reaching the surface during annealing (with corresponding diffraction pattern).

Fig. 4. Krypton bubbles in restored silicon matrix. The arrow points at the entrance surface (⟨110⟩ projection).

4. Discussion and conclusions

It was shown that the bombardment of silicon targets carried out with heavy ions to the high doses used in the experiment resulted in total amorphization of surface layers, as was expected. However, the swelling of the damaged layer which was stated in the case of D_3 implant needs a better understanding. A possible explanation may be an additional effect of a layer broadening by the dose increase *plus* the observed krypton bubble nucleation owing to the high deposited Kr concentration over the solubility limit in amorphous Si phase.

Both annealing procedures, the conventional and by laser pulses (the latter starting with short melting reaching a depth of undamaged bulk material) resulted in epitaxial recrystallization of surface layers. The observed secondary defect structures and differences between them are certainly a matter of solid vs. liquid phase epitaxial regrowth and are especially influenced by behaviour of impurity atoms during the processes.

As krypton is essentially insoluble in solids the Kr precipitation is the most expected (and actually observed) effect during the restoration of Si crystalline structure. For such high doses the bubbles created at around a depth of the highest Kr concentration (approximately R_p) may act as a barrier and stop the incoming front of microtwins as became evident at least in the case of D_3/F. Though for the two lower doses information about the orientation of underlying substrate is not completely lost above the depth of R_p, regrowth on furnace annealing is also heavily disturbed at the surface. As we suppose it is probably caused by the agglomeration of Kr atoms (in the form of overpressurized gaseous or liquid bubbles) hoping to out-diffuse but trapped by a very resistive oxide film formed on the surfaces during processing (see the micrograph in Fig. 2).

This artifactually introduced "boundary condition" (that is: the surface is impermeable to krypton) which modify the process of recrystallization in a furnace, is not fulfilled at all during the applied laser treatment. In this case Kr concentration profiles are affected by both the diffusion in the liquid phase and the segregation of impurities at the moving melt-front during the solidification [8]. Furthermore, Kr diffusivity in the melt is several orders of magnitude higher than it is in the solid. Following these general facts one can suppose that a better quality recrystallization on laser annealing is achieved at an expense of the significant reduction of deposited Kr concentration by evaporation and some loss of surface layer.

Finally, it is proper to compare the present results with our previous TEM observations of ⟨100⟩-oriented Si wafers which had been implanted at RT with medium doses of Kr^+ ions of 300 keV energy [9]. It was concluded then that implantation to the doses of 5×10^{13} and 5×10^{14} i/cm^2 led, respectively, to incomplete and complete amorphization of the entire bombarded region, whereas for the intermediate dose 1×10^{14} i/cm^2 a continuous amorphous layer was just beginning to be formed at a depth of 0.8 R_p. Instead of microtwins reported above, small interstitial Frank dislocation loops and rod-like defects were found to be predominant secondary defects created during subsequent SPE regrowth of the damaged layers. Creation of just these kinds of structural defects upon annealing and absence of twinning was certainly a matter of different orientation of recrystallization front (i.e. ⟨100⟩ instead of ⟨111⟩).

Perhaps the most interesting result of medium-dose studies was the possibility to detect early nucleation of polyhedrally-shaped Kr precipitates of approx. 5 nm or less in size (only in the case of the 5×10^{14} i/cm^2 dose). Dark field imaging observations indicated that probably a large fraction of these bubbles contained solid krypton precipitates [10]. Formation of such small solid phase bubbles upon inert gas implantation was reported by several research groups (e.g [11]). Following the theoretical considerations [12], at room temperature the medium and large

sized bubbles like these observed during the present high-dose experiments can be filled only with gas or fluid.

Acknowledgments

The author would like to thank Prof. J. Auleytner for his helpful comments and critical reading of the manuscript, and to Dr. H. Bartsch for stimulating discussion and his assistance in using the high-voltage electron microscope.

*

This work was partially sponsored by the Committee for Scientific Research (No. 935/2/91).

References

[1] A.G. Cullis, in: *Defects in Semiconductors*, Eds. J. Narayan, T.Y. Tan, North-Holland, New York 1981, p. 393.

[2] J.F. Gibbons, W.S. Johnson, S.W. Mylroie, *Projected Range Statistics*, Dowden, Hutchison and Ross, Inc., Stroudsburg (Pennsylvania) 1975.

[3] C.R. Booker, R. Stickler, *Br. J. Appl. Phys.* **13**, 446 (1962).

[4] J.C. Bravman, R. Sinclair, *J. Electron Microsc.* **1**, 53 (1984).

[5] J. Washburn, in: *Defects in Semiconductors*, Eds. J. Narayan, T.Y. Tan, North-Holland, New York 1981, p. 209.

[6] S. Mader, in: *Ion Implantation Techniques*, Eds. H. Ryssel, H. Glawischnig, Springer Verlag, Berlin 1982, p. 301.

[7] D.W. Pashley, M.J. Stowell, *Philos. Mag.* **8**, 1605 (1963).

[8] W. Schwarzott, *Forsch. Ing.-Wes.* **38**, 165 (1972).

[9] J. Morawiec, in: *Ion Implantation and Ion Beam Equipment*, Eds. D.S. Karpuzov, I.V. Katardjiev, S.S. Todorov, World Scientific, Singapore 1991, p. 28.

[10] J. Morawiec, unpublished.

[11] C. Templier, H. Garem, J.P. Riviere, *Philos. Mag. A* **53**, 667 (1986).

[12] K.F. Niebel, J.A. Venables, in: *Rare Gas Solids*, Eds. M.L. Klein, J.A. Venables, Academic Press, London 1976, p. 558.